scientific reports

OPEN

The impacts of shape factor and heat transfer on two-phase flow of nano and hybrid nanofluid in a saturated porous medium

P. V. Ananth Subray[1], B. N. Hanumagowda[1], S. V. K. Varma[1] & Mohammad Hatami[2,3]✉

The focus of this article is to obtain the effect of shape factor of the hybrid nanoparticles on the convective heat and mass transference of two immiscible fluids in an inclined duct by employing the perturbation technique. The hybrid nanoparticle of Carbon Nanotube & Sodium alginate is being used with Silicon oil as the base fluid to study the heat and mass phenomena due to the soret effect, viscous dissipation, Darcy and Thermal diffusion. The physical flow problem is then modelled into a set of differential equations. The system of equations is solved analytically to obtain various graphical and numerical results for analyzing the impact of various material parameters on velocity and thermal field. The heat transfer rate and skin friction analysis for the flow dynamics are also investigated. It is observed that the shape factor enhances the fluid flow and temperature distribution. In specific lamina shape particles have better performance comparatively, significance of the soret number can also be observed.

List of symbols

ω	Angle of inclination
Br	Brinkman number
Sc	Schmid number
ST	Soret parameter
Grl	Thermal grashof number
Grc	Solutal grashof number
ϕ	Solid volume fraction
σ	Porous medium parameter
g	Gravitational force
Nu	Nusselt number
τ	Skin friction
ρ	Density of fluid
θ	Dimensionless temperature
ψ	Dimensionless concentration
κ	Thermal conductivity of a fluid
μ	Dynamics viscosity (m^2s^{-1})
ν	Kinematic viscosity (m^2s^{-1})
β	Thermal expansion coefficient
ϕ	Porosity of the porous media

Subscripts

nf	Nanofluid
hnf	Hybrid nanofluid
f	Base fluid
s	Solid particle

[1]School of Applied Sciences, REVA University, Bengaluru, Karnataka, India. [2]Mechanical Engineering Department, Ferdowsi University of Mashhad, Mashhad, Iran. [3]Mechanical Engineering Department, Esfarayen University of Technology, Esfarayen, North Khorasan, Iran. ✉email: m-hatami@um.ac.ir; m.hatami@xjtu.edu.cn

In recent days, the strive to enhance the thermal conductivity of fluids is more and new kinds of fluids namely nanofluids have been developed to fulfil the needs[1–5]. Nanoparticles are colloidal systems with the size of the particles to be 10^{-9}. Industries such as lubricants, hydraulic oils, food industry, solar collectors etc.[6–12] attract these kinds of fluid which have special properties. Although nanofluids fulfil the needs of these industries in recent days there is a need for better fluids which enhances the heat transfer rates[13–16]. This works deals with the study of the effect of hybrid nanofluids as a lubricant or hydraulic fluid which has better performance than the existing class of fluids.

Hybrid nanofluid is extensively used in various heat transfer applications which include heat exchangers, heat sinks, heat pipes, photovoltaic modules, natural convection enclosures, refrigeration systems, jet impingement cooling, boiling, and thermal energy storage systems. By considering these applications Jana et al.[17] experimentally obtained the hybrid nanofluids by appending a couple of diverse nanoparticles in the base fluid, as they are a pioneering class of fluid. They noticed the enhancement of heat transfer in these fluids by adding both single and hybrid Nanoparticles. Niihara[18] examined the composite layer of nanoparticle and concluded that the composite layer not only improves the thermal conductivity but also they enhance the mechanical properties. Chamkha et al.[19] recorded the heat transfer characteristic of the fluid flow with copper and aluminium oxide filled with water in a porous cavity. The study of hybrid nanofluids in various geometries[20–24] is studied due to the applications from various researchers.

Many recent studies show the shape factor of the nanoparticle plays a major role in the change in the thermophysical properties with the expected results[25]. Sobamowo[26] examined the shape factor effect in hybrid nanofluids by varying the values of the Prandtl number. They noticed the desired outcome is obtained in a lamina shape. Hussain et al.[27] investigated the effect of shape factors in nanoparticles with thermal radiation. Muneeshwaran et al.[28] examined the role of hybrid nanofluids in the enhancement of heat transfer and their applications in industries.

Another method to enhance the heat transfer rate is by equipping the permeable medium[29]. For example, the use of metal-based porous materials in channel and heat exchangers. The method of using hybrid nanofluid and permeable medium has been investigated by many researchers[30–32]. As permeable media provides more area of contact between the surfaces. Also, hybrid nanofluids improve thermal conduction. Therefore, combining permeable medium and hybrid nanofluids can enhance the productivity of the thermal system. Anwar et al. studied the effect of a porous medium in two-phase flow for electrically conducting and non-conducting fluids[33].

The fluid flow in two regions is due to the drag force[34] of the shear stress by fluid flowing next it to, which has a wide range of applications such as oil–gas mixtures, evaporators, boilers, condensers, submerged combustion systems, sewerage treatment plants, air-conditioning and refrigeration plants, and cryogenic plants. The study of two immiscible fluids in different geometries was deliberated by Khaled[35], Umavathi[36] and Chen[37]. Two immiscible fluids with one conducting and another non-conducting property were considered by Malashetty et al.[38]. The investigation of two-phase flow in a permeable medium with an electrically conducting and heat-generating or absorbing was carried out by Chamkha[39]. The heat transfer of a two-phase unsteady flow of nanofluids with magnetic properties was investigated by Sheikholeslami et al.[40] and studied the variations caused due to the haphazard motion of the particle and soret effect using the numerical technique. Some of the recent study related to two-phase flow is carried out[41–45] in the presence of Casson and micropolar fluids.

From an overview of available literature, very sparse research is carried out related to the hybridization of Carbon Nanotube & Sodium alginate in Silicon oil along with consideration of the shape factor, even though they are widely used as lubricating oil and hydraulic fluid. Hence this study focuses on studying them along with the soret effect and permeable medium in a two-phase flow.

Problem description

The physical configuration is illustrated in Fig. 1. A steady, laminar, incompressible, fully developed and mixed convective flow of viscous incompressible Hybrid nanofluid along an infinitely long inclined plate with an acute angle Θ considered, with an x-axis is along the plate with a distance of h between the plates. The left boundary walls are kept at a T_{w2} and the right wall is kept at T_{w1} a temperature where $T_{w1} \geq T_{w2}$. We have assumed the density to be persistent everywhere except when it is multiplied by gravity i.e., Oberbeck-Boussinesq approximation[46]. The flow is assumed to be due to the buoyancy and pressure forces.

We consider Hybrid nanofluid in region-1 $(-h \leq y \leq 0)$ and Nanofluid in region-2 $(0 \leq y \leq h)$. We have considered Silicon oil as the base fluid and Carbon Nanotube & Sodium alginate as nanoparticles. Silicon oil is used as a cooling and insulting liquid for transformers and other electrical equipment. The shape factor of the nanoparticle is considered in our study which is presented in Table 1.

With these assumptions, Tiwari and Das[49] model for nanofluids and Darcy law[50] which excludes the porous medium inertia effects[51,52] as the flow is unidirectional and function of y. Governing equations of motion, energy and concentration become (Ghasemi and Aminossadati[53], Muthtamilselvan et al.[54], Vajravelu et al.[55]):

Region-1.

$$\mu_{hnf}\frac{d^2u_1}{dy^2} + \left(\rho_{hnf}g\beta_{hnf}\right)(T_1 - T_{w2})\cos(\Theta) + \left(\rho_{hnf}g\beta_{hnc}\right)(C_1 - C_{w2})\cos(\Theta) - \frac{\partial p}{\partial x} = 0 \tag{1}$$

$$k_{hnf}\frac{d^2T_1}{dy'^2} + \mu_{hnf}\left(\frac{du_1}{dy}\right)^2 = 0 \tag{2}$$

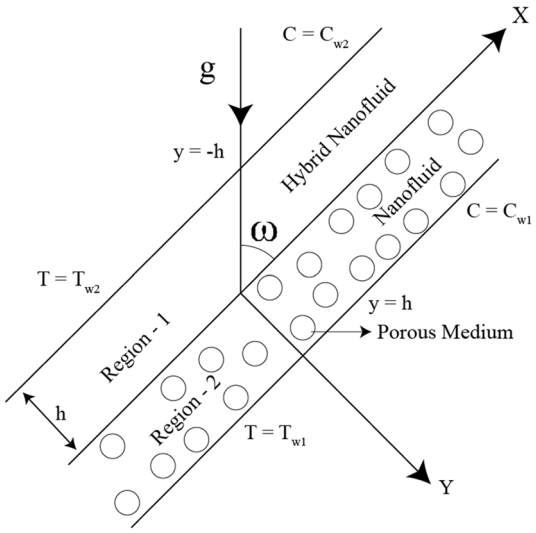

Figure 1. Physical model.

Shape of the nanoparticles	Shape factor (q)
Brick	3.7
Blade	8.6
Laminar	16.1576

Table 1. Values of the nanoparticle's Shape factor[47,48].

$$D_1 \frac{d^2 c_1}{dy^2} + D_T \frac{d^2 T_1}{dy^2} = 0 \tag{3}$$

Region-2.

$$\mu_{nf} \frac{d^2 u_2'}{dy'^2} + \left(\rho_{nf} g \beta_{nf}\right)(T_2 - T_{w2}) \cos(\Theta) + \left(\rho_{nf} g \beta_{nc}\right)(C_2 - C_{w2}) \cos(\Theta) - \frac{\mu_{nf}}{\kappa} u_2' - \frac{\partial p}{\partial x} = 0 \tag{4}$$

$$k_{nf} \frac{d^2 T_2}{dy'^2} + \mu_{nf} \left(\frac{du_2'}{dy'}\right)^2 + \frac{\mu_{nf}}{\kappa} u_2'^{\,2} = 0 \tag{5}$$

$$D_2 \frac{d^2 c_2}{dy^2} + D_T \frac{d^2 T_2}{dy^2} = 0 \tag{6}$$

The above-defined governing equations for velocities (1) and (4) require four conditions to solve. Which are drawn from the assumptions made at the walls and by equating the interface constraints. Similarly, the boundary constraints for temperature and concentration are obtained. Which is of the form:

$$u_1(-h) = 0,\ u_1(0) = u_2(0),\ \mu_{hnf} \frac{du_1(0)}{dy} = \mu_{nf} \frac{du_2(0)}{dy},\ u_2(h) = 0 \tag{7}$$

$$T_1(-h) = T_{w2},\ T_1(0) = T_2(0),\ k_{hnf} \frac{dT_1(0)}{dy'} = k_{nf} \frac{dT_2(0)}{dy'},\ T_2(h) = T_{w1} \tag{8}$$

$$c_1(-h) = 0,\ c_1(0) = c_2(0),\ \frac{dc_1(0)}{dy} = \frac{D_2}{D_1} \frac{dc_2(0)}{dy},\ c_2(h) = 1 \tag{9}$$

The effective characteristics of hybrid nanofluids and Mono nanofluids considered in our study are listed in Table 2. Where ϕ_1 and ϕ_2 are the solid volume fraction of the particles. K_{nf} and K_{hnf} are the thermal conductivity with the shape factor q according to Maxwell[56], Brinkman model for the viscosity is considered[57]. The subscripts

Properties	Mono nanofluid	Hybrid nanofluid
Density	$\rho_{nf} = (1-\phi)\rho_f + \phi\rho_s$	$\rho_{hnf} = [(1-\phi_1)\rho_f + \phi_1\rho_{s1}](1-\phi_2) + \rho_{s2}\phi_2$
Heat capacity	$(\rho C_p)_{nf} = (1-\phi)(\rho C_p)_f + \phi(\rho C_p)_s$	$(\rho C_p)_{hnf} = (\rho C_p)_f(1-\phi_2)\left[(1-\phi_1) + \phi_1\frac{(\rho C_p)_{s1}}{(\rho C_p)_f}\right] + \phi_2(\rho C_p)_{s2}$
Dynamic viscosity[57]	$\mu_{nf} = \frac{\mu_f}{(1-\phi)^{2.5}}$	$\mu_{hnf} = \frac{\mu_f}{\sqrt{(1-\phi_1)^5(1-\phi_2)^5}}$
Thermal conductivity[56]	$K_{nf} = K_f\left\{\frac{K_{s1}+(q-1)K_f-(q-1)\phi(K_f-K_{s1})}{K_{s1}+(q-1)K_f+\phi(K_f-K_{s1})}\right\}$	$k_{hnf} = k_{hf}\left[\frac{(k_{s2}+(q-1)k_{nf})-(q-1)\phi_{n2}(k_{nf}-k_{s2})}{(k_{s2}+(q-1)k_{nf})+\phi_{n2}(k_{nf}-k_{s2})}\right]$

Table 2. Thermophysical properties of nanoparticle and hybrid nanoparticle.

hnf, *nf*, *s*, 1 and 2 represents the hybrid nanofluid, nanofluid, solid nanoparticle, first nanoparticle and second nanoparticle respectively.

To convert the Eqs. (1)–(9) to dimensionless form we use the following terms:

$$y = \frac{y'}{h}, \quad u_i = u_i'\left(\frac{\rho_f}{\mu_f}\right)h, \quad \theta_i = \frac{T_i - T_{w2}}{T_{w1} - T_{w2}}, Grl = \frac{g\beta_f\left(T_{w1} - T_{w2}\right)h^3}{v_f^2}$$

$$Grc = \frac{g\beta_c\left(C_{w1} - C_{w2}\right)h^3}{v_f^2} \quad \sigma = \frac{h}{\sqrt{\kappa}}, P = -\frac{\rho_f h^3}{\mu_f^2}\frac{\partial p}{\partial x}, v_f = \frac{\mu_f}{\rho_f}$$

$$S_T = \frac{D_T}{\upsilon}\frac{\left(T_{w2} - T_{w1}\right)}{\left(c_{w2} - c_{w1}\right)}, \; S_c = \frac{\upsilon}{D_2}, \; \psi_i = \frac{C_i - C_{w2}}{C_{w1} - C_{w2}} \tag{10}$$

Substituting Eq. (10) into Eqs. (1)–(9) and after dropping the asterisks we obtain the following non-dimensional form of the governing equations considering Supplementary Information for constant parameters.

Region-1.

$$\frac{d^2u_1}{dy^2} + A_1 Grl\theta_1 + A_2 Grc\psi_1 - P_2 = 0 \tag{11}$$

$$\frac{d^2\theta_1}{dy^2} + BrA_4\left(\frac{du_1}{dy}\right)^2 = 0 \tag{12}$$

$$\frac{1}{S_c}\frac{d^2\psi_1}{dy^2} + S_T\frac{d^2\theta_1}{dy^2} = 0 \tag{13}$$

Region II.

$$\frac{d^2u_2}{d^2y} + (A_5 Grl\theta_2) + (A_6 Grc\psi_2) - \sigma^2 u_2 + P_1 = 0 \tag{14}$$

$$\frac{d^2\theta_2}{dy^2} + A_7 B_r\left\{\left(\frac{du_2}{dy}\right)^2 + \sigma^2 u_2^2\right\} = 0 \tag{15}$$

$$\frac{1}{S_c}\frac{d^2\psi_2}{dy^2} + S_T\frac{d^2\theta_2}{dy^2} = 0 \tag{16}$$

The non-dimensional boundary and interface conditions are

$$\left.\begin{aligned} &u_1(-1)=0\,,\ u_1(0)=u_2(0)\,,\frac{du_1(0)}{dy}=\frac{\mu_{nf}}{\mu_{hnf}}\frac{du_2(0)}{dy}\,,u_2(1)=0\\ &\theta_1(-1)=0\,,\ \theta_1(0)=\theta_2(0)\,,\frac{d\theta_1(0)}{dy}=\frac{k_{nf}}{k_{hnf}}\frac{d\theta_2(0)}{dy}\,,\theta_2(1)=1\\ &\psi_1(-1)=0\,,\ \psi_1(0)=\psi_2(0)\,,\frac{d\psi_1(0)}{dy}=\frac{D_2}{D_1}\frac{d\psi_2(0)}{dy}\,,\ \psi_2(1)=1 \end{aligned}\right\} \tag{17}$$

Solution method. The Governing equations of assumed flow replica & respective boundary conditions are defined in Eqs. (11)–(17), which are ordinary nonlinear coupled equations. Where the Brinkman number is assumed to be perturbation constant to overcome limitations of the assumed analytical technique. Brinkman number has lots of practical applications when the value ranges between zero and one. By considering the special properties of a Brinkman number, we have calculated the approximations of temperature, concentration and velocity:

$$u_i(y)=u_{i0}(y)+Bru_{i1}+(Br)^2u_{i2}(y)+\ldots \tag{18}$$

$$\theta_i(y)=\theta_{i0}(y)+Br\theta_{i1}+(Br)^2\theta_{i2}(y)+\ldots \tag{19}$$

$$\psi_i(y)=\psi_{i0}(y)+Br\psi_{i1}+(Br)^2\psi_{i2}(y)+\ldots \tag{20}$$

Inputting the Eqs. (18)–(20) into (12)–(18) and equating the coefficients of the like powers of Br to zero, we obtain the following equations:

Zeroth order equations. *Region-1.*

$$\frac{d^2u_{10}}{dy^2}+A_1Grl\theta_{10}+A_2Grc\psi_{10}-P_2=0 \tag{21}$$

$$\frac{d^2\theta_{10}}{dy^2}=0 \tag{22}$$

$$\frac{1}{S_c}\frac{d^2\psi_{10}}{dy^2}+S_T\frac{d^2\theta_{10}}{dy^2}=0 \tag{23}$$

Region-2.

$$\frac{d^2u_{20}}{d^2y}+(A_5Grl\theta_{20})+(A_6Grc\psi_{20})-\sigma^2u_{20}+P_1=0 \tag{24}$$

$$\frac{d^2\theta_{20}}{dy^2}=0 \tag{26}$$

$$\frac{1}{S_c}\frac{d^2\psi_{20}}{dy^2}+S_T\frac{d^2\theta_{20}}{dy^2}=0 \tag{26}$$

The boundary and interface conditions for zeroth order are

$$\left.\begin{aligned} &u_{10}(-1)=0,u_{10}(0)=u_{20}(0),\frac{du_{10}(0)}{dy}=\frac{\mu_{nf}}{\mu_{hnf}}\frac{du_{20}(0)}{dy},u_{20}(1)=0\\ &\theta_{10}(-1)=0,\theta_{10}(0)=\theta_{20}(0),\frac{d\theta_{10}(0)}{dy}=\frac{k_{nf}}{k_{hnf}}\frac{d\theta_{20}(0)}{dy},\theta_{20}(1)=1\\ &\psi_{10}(-1)=0,\psi_{10}(0)=\psi_{20}(0),\frac{d\psi_{10}(0)}{dy}=\frac{D_2}{D_1}\frac{d\psi_{20}(0)}{dy},\psi_{20}(1)=1 \end{aligned}\right\} \tag{27}$$

First-order equations. *Region-1.*

$$\frac{d^2u_{11}}{dy^2} + A_1 Grl\theta_{11} + A_2 Grc\psi_{11} = 0 \tag{28}$$

$$\frac{d^2\theta_{11}}{dy^2} + A_4\left(\frac{du_{10}}{dy}\right)^2 = 0 \tag{29}$$

$$\frac{1}{S_c}\frac{d^2\psi_{11}}{dy^2} + S_T\frac{d^2\theta_{11}}{dy^2} = 0 \tag{30}$$

Region-2.

$$\frac{d^2u_{21}}{d^2y} + (A_5 Grl\theta_{21}) + (A_6 Grc\psi_{21}) - \sigma^2 u_{21} + P_1 = 0 \tag{31}$$

$$\frac{d^2\theta_{21}}{dy^2} + A_7\left\{\left(\frac{du_{20}}{dy}\right)^2 + \sigma^2 u_{20}^2\right\} = 0 \tag{32}$$

$$\frac{1}{S_c}\frac{d^2\psi_{21}}{dy^2} + S_T\frac{d^2\theta_{21}}{dy^2} = 0 \tag{33}$$

The boundary and interface conditions for the first order are

$$\left.\begin{aligned} &u_{11}(-1) = 0\,,\ u_{11}(0) = u_{21}(0)\,, \frac{du_{11}(0)}{dy} = \frac{\mu_{nf}}{\mu_{hnf}}\frac{du_{21}(0)}{dy}\,, u_{21}(1) = 0\\ &\theta_{11}(-1) = 0\,,\ \theta_{11}(0) = \theta_{21}(0)\,, \frac{d\theta_{11}(0)}{dy} = \frac{k_{nf}}{k_{hnf}}\frac{d\theta_{21}(0)}{dy}\,, \theta_{21}(1) = 0\\ &\psi_{11}(-1) = 0\,,\ \psi_{11}(0) = \psi_{21}(0)\,, \frac{d\psi_{11}(0)}{dy} = \frac{D_2}{D_1}\frac{d\psi_{21}(0)}{dy}\,,\ \psi_{21}(1) = 0 \end{aligned}\right\} \tag{34}$$

Equations (21)–(34) are solved by integrating and using the respective boundary conditions we get the following solution. The intermediate steps are vomited as it's a simple integration and simplification.

Temperature.

$$\theta_1 = c_1 y + c_2 + Br\left(L_5\frac{y^6}{120} + L_6\frac{y^5}{20} + L_7\frac{y^4}{12} + L_8\frac{y^3}{6} + L_{911}\frac{y^2}{2} + c_{11}y + c_{12}\right) \tag{35}$$

$$\theta_2 = c_3 y + c_4 - Br\left(A_7\left[\begin{aligned} &\frac{L_9}{4\sigma^2}\mathrm{Cosh}2\sigma y + \frac{L_{10}}{4\sigma^2}\mathrm{Sinh}2\sigma y + \frac{L_{11}}{\sigma^3}y\sigma\,\mathrm{Sinh}\sigma y + \frac{L_{12}}{\sigma^3}y\sigma\,\mathrm{Cosh}\sigma y + L_{17}\frac{y^2}{2}\\ &+\left(\frac{L_{14}}{\sigma} - \frac{L_{12}}{\sigma^2} - \frac{L_{12}}{\sigma^2}\right)\frac{1}{\sigma}\mathrm{Sinh}\sigma y + \left(\frac{L_{13}}{\sigma} - \frac{L_{11}}{\sigma^2} - \frac{L_{11}}{\sigma^2}\right)\frac{1}{\sigma}\mathrm{Cosh}\sigma y + L_{15}\frac{y^4}{12} + L_{16}\frac{y^3}{6}\end{aligned}\right] + c_{21}y + c_{22}\right) \tag{36}$$

Velocity.

$$u_1 = \left(L_1\frac{y^3}{6} + L_2\frac{y^2}{2} + b_{11}y + b_{12}\right) + Br\left(\frac{L_{32}}{56}y^8 + \frac{L_{33}}{42}y^7 + \frac{L_{34}}{30}y^6 + \frac{L_{35}}{20}y^5 + \frac{L_{36}}{12}y^4 + \frac{L_{37}}{6}y^3 + \frac{L_{38}}{2}y^2 + c_{51}y + c_{52}\right)$$

$$u_2 = \left(\begin{matrix} b_{21}\mathrm{Cosh}\sigma y + b_{22}\mathrm{Sinh}\sigma y\\ +L_3 y + L_4\end{matrix}\right) + Br\left(\begin{aligned} &c_{61}\mathrm{Cosh}\sigma y + c_{62}\mathrm{Sinh}\sigma y + L_{39}\mathrm{Cosh}2\sigma y + L_{40}\mathrm{Sinh}2\sigma y\\ &+L_{41}\left(\frac{y^2}{2}\mathrm{Cosh}\sigma y - \frac{y}{2\sigma}\mathrm{Sinh}\sigma y\right) + L_{42}\left(\frac{y^2}{2}\mathrm{Sinh}\sigma y - \frac{y}{2\sigma}\mathrm{Cosh}\sigma y\right)\\ &+L_{43}\frac{y}{2\sigma}\mathrm{Cosh}\sigma y + L_{44}\frac{y}{2\sigma}\mathrm{Sinh}\sigma y + L_{45}\left(y^4 + \frac{12}{\sigma^2}y^2 + \frac{24}{\sigma^4}\right)\\ &+L_{46}\left(y^3 + \frac{6}{\sigma^2}y\right) + L_{47}\left(y^2 + \frac{2}{\sigma^2}\right) + L_{48}y + L_{49}\end{aligned}\right) \tag{37}$$

Concentration.

$$\psi_1 = c_5 y + c_6 + Br\left(L_{18}y^6 + L_{19}y^5 + L_{20}y^4 + L_{21}y^3 + L_{22}y^2 + c_{31}y + c_{32}\right)$$

$$\psi_2 = c_7 y + c_8 + Br\begin{pmatrix} L_{23}\mathrm{Cosh}2\sigma y + L_{24}\mathrm{Sinh}2\sigma y + L_{25}y\sigma\,\mathrm{Sinh}\sigma y + L_{26}y\sigma\,\mathrm{Cosh}\sigma y + L_{27}\mathrm{Sinh}\sigma y \\ + L_{28}\mathrm{Cosh}\sigma y + L_{29}y^4 + L_{30}y^3 + L_{31}y^2 + c_{41}y + c_{42} \end{pmatrix} \quad (38)$$

Derived quantities. Nusselt number: It is the rate of heat transfer at the right & left plate.

$$(Nu)_{y=-1} = \left(\frac{d\theta_1}{dy}\right)_{y=-1} = c_1 + Br\left(c_{11} - \frac{L_5}{20} + \frac{L_6}{4} - \frac{L_7}{3} + \frac{L_8}{2} - L_{911}\right) \quad (39)$$

$$(Nu)_{y=1} = -\left(\frac{d\theta_2}{dy}\right)_{y=1} = -c_1 - Br\left(c_{11} + \frac{L_5}{20} + \frac{L_6}{4} + \frac{L_7}{3} + \frac{L_8}{2} + L_{911}\right) \quad (40)$$

Skin friction: It is friction between the fluid and the surface of a solid for fluid in relative motion.

$$(\tau)_{y=-1} = \left(\frac{du_1}{dy}\right)_{y=-1} = \left(b_{11} + \frac{L_1}{2} - L_2\right) + Br\left(c_{51} - \frac{L_{32}}{7} + \frac{L_{33}}{6} - \frac{L_{34}}{5} + \frac{L_{35}}{4} - \frac{L_{36}}{3} + \frac{L_{37}}{2} - L_{38}\right) \quad (41)$$

$$(\tau)_{y=1} = -\left(\frac{du_2}{dy}\right)_{y=1} = -\left(b_{11} + \frac{L_1}{2} + L_2\right) - Br\left(c_{51} + \frac{L_{32}}{7} + \frac{L_{33}}{6} + \frac{L_{34}}{5} + \frac{L_{35}}{4} + \frac{L_{36}}{3} + \frac{L_{37}}{2} + L_{38}\right) \quad (42)$$

Results and discussion

An analytical method is used to calculate the two-layered hybrid nanofluid flow by employing regular perturbation techniques for numerous germane parameters. The flow is formulated by considering Silicon oil as a base fluid and CNT and $(C_6H_8O_6)_n$ nanoparticles. Graphical representation of the solution is given by graphs and Eqs. (2)–(19) which furnish special features of saturated hybrid nanofluid in two-immiscible fluids in presence of soret effect and angle of inclination.

Figure 2a represents the change in velocity with Grl and shape factor. For increasing values of Gr and an increment in the velocity of fluid flow can be observed, maximum can be observed in region-1 and then reduces at region-2. Region-1 consists of a hybrid nanofluid and region-2 with nanofluid in the occurrence of a saturated permeable medium and hence that difference in the velocity is noticed. It can be noticed that the velocity for the Laminar shape is greater than the blade shape and brick-shaped nanoparticles.

The same results are observed for temperature in Fig. 2c. Figure 2b and d depicts the change in velocity & temperature due to the influence of Gr and solid volume fraction. We have considered the ϕ_2 to be zero and obtained Fig. 2b with this the region-1 reduces to the Nanofluid and region-2 reduces to clear fluid in the presence of a saturated porous medium. It can be observed that the Laminar shaped nanoparticle has a higher velocity in region-1 and lesser in region-2 to due the porosity of the material.

Figure 3a and b shows the effect of Br on the velocity of the fluid flow. In Fig. 3a it is spotted that velocity increment is more prevalent in region-1 than region-2 and Fig. 3b shows that the velocity is higher in the presence of nanofluid than in the clear fluid. It is obtained by keeping ϕ_2 to zero. From Figure 3c and d it can be noticed that the temperature increases by incrementing the values of Br. The increment of fluid flow and temperature can be witnessed due to the enhancement of the thermal energy produced due to viscous dissipation. The dissipation of upwards fluid temperature and subsequently the buoyancy force. Therefore, an increment in the buoyancy force upsurges the fluid flow in the upward direction. From these graphs, it can be noticed the velocity and temperature are higher for laminar shape nanoparticles followed by blade and brick shape.

Figure 4a–d demonstrates the effect of the angle of inclination on fluid velocity and temperature for both regular ($\phi = 0$) and nanofluid ($\phi \neq 0$). It can be seen that the velocity of the fluid is decreased by incrementing the angle and it can also be observed that for velocity is higher for the hybrid nanofluid than for the mono nanofluid. Whereas the temperature is wise versa it is due to the increase of amplification and driving force acting on the fluid. Also, the shape of the nanoparticle chosen plays an important role and is observed maximum for lamina-shaped particles.

The influence of the porosity medium parameter (σ) on velocity and temperature distribution can be seen in Fig. 5a–d for CNT and cobalt ferrite in silicon oil. It is perceived that the increase σ reduces the fluid flow and temperature. Whereas velocity is observed to be greater in region-1 than in region-2. Also, when ϕ_2 is kept at zero it can be observed velocity is higher for smaller values σ and then reduces in the clear fluid region. The Laminar shaped particles have more velocity and temperature than others. It is quite seeming to be unusual, but the friction is caused by flow and porous media so thermal conductivity raises which results in enhancement of temperature can be observed in the above figure and the other trends are the same as mentioned for velocity.

Figure 6a and b are the plots of concentration for various values of Sc and shape factor. Comparing the arches from the figure, it can be observed that an increment in Schmidt number declines the concentration at all the points. This is due to the concentration buoyancy effect which reduces fluid flow. Further concentration can

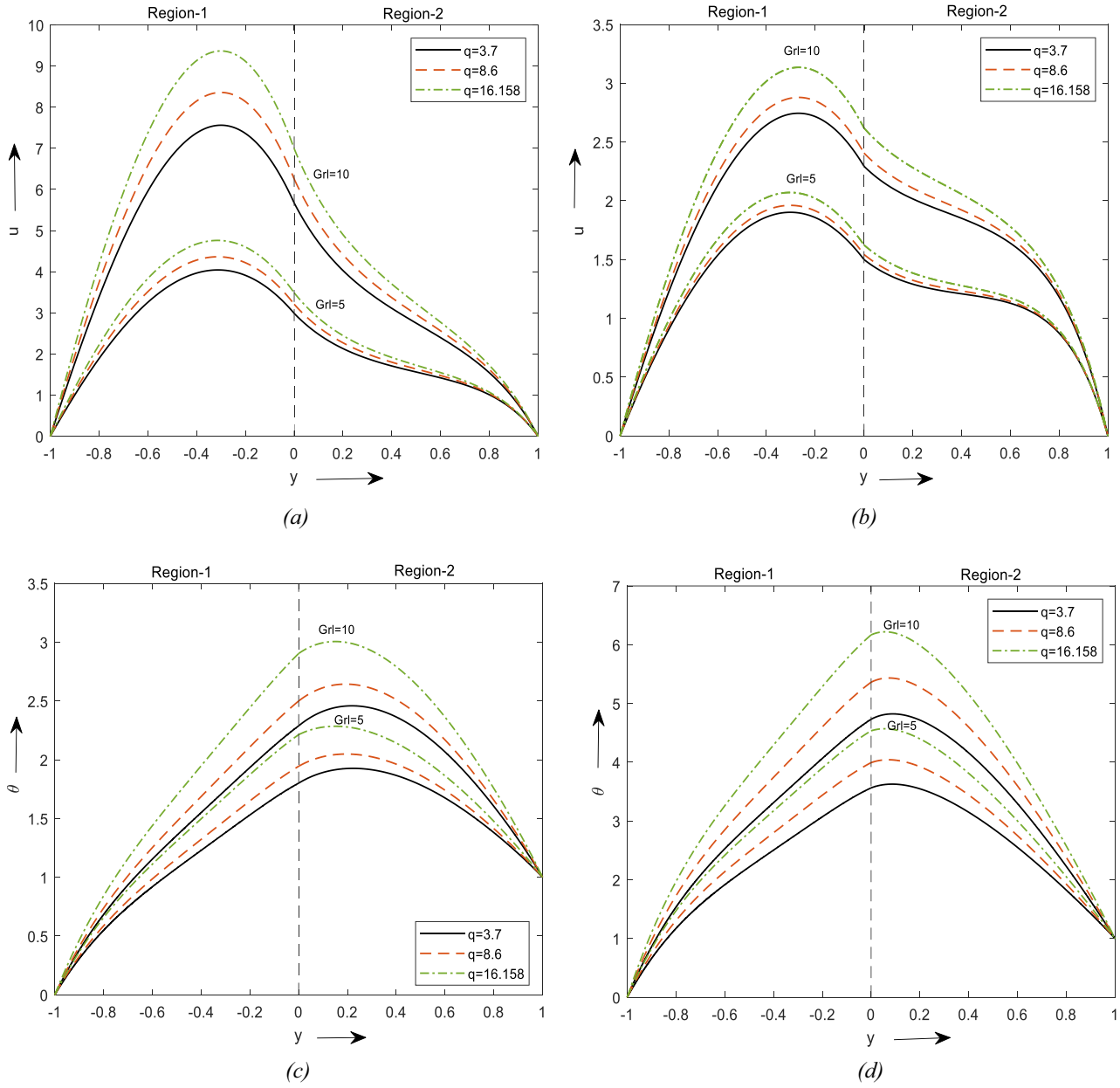

Figure 2. Velocity profiles for different values of Thermal Grashof number. (**a**) For two different values of ϕ. (**b**) for a value of ϕ. Temperature profiles for different values of Br. (**c**) For two different values of ϕ. (**d**) For a value of ϕ.

be reduced by employing laminar-shaped nanoparticles. Similar phenomena can be observed in Fig. 6b in the absence of a hybrid nanofluid.

Figure 7a and b shows the graph for increasing values of thermophoresis to concentration. It depicts the impact of temperature gradient on mass diffusion. In graphs, an increase in Thermophoresis provokes a rise in temperature and fluid concentration decays. Thermophoresis is observed to be utmost in when nanoparticles region and minimal in the hybrid nanofluid region. Concentration is observed to be maximum for the Brick shaped particles which are followed by Blade and laminar. A similar trend is observed when region-1 is considered a nanofluid region and other to be a clear fluid region.

Figure 8 depicts the Nu and Sk for different values of Grc and GrL at the plates. Figure 8a is plotted for the nusselt number at $y = -1$ and Figure 8b at $y = 1$, Figure 8c is plotted for skin friction number at $y = -1$ and Figure 8d at $y = 1$. From these graphs, an increasing value of Grc and GrL, a rise in the nusselt number is observed. In Figure 8a when the GrL is kept to be constant and for increasing values of Grc, the rate of heat transfer reaches the peak gradually at $y = -1$. From Figure 8b we can notice that heat transfer decrease gradually at the right plate ($y = 1$). The results can be analysed by keeping the Grc Constant and varying GrL.

To find the combined effect of Br and porous media parameters on heat transfer rate and resistance to the flow, the Nusselt number and Skin friction graphs are plotted, which are displayed in Fig. 9a–d respectively. It

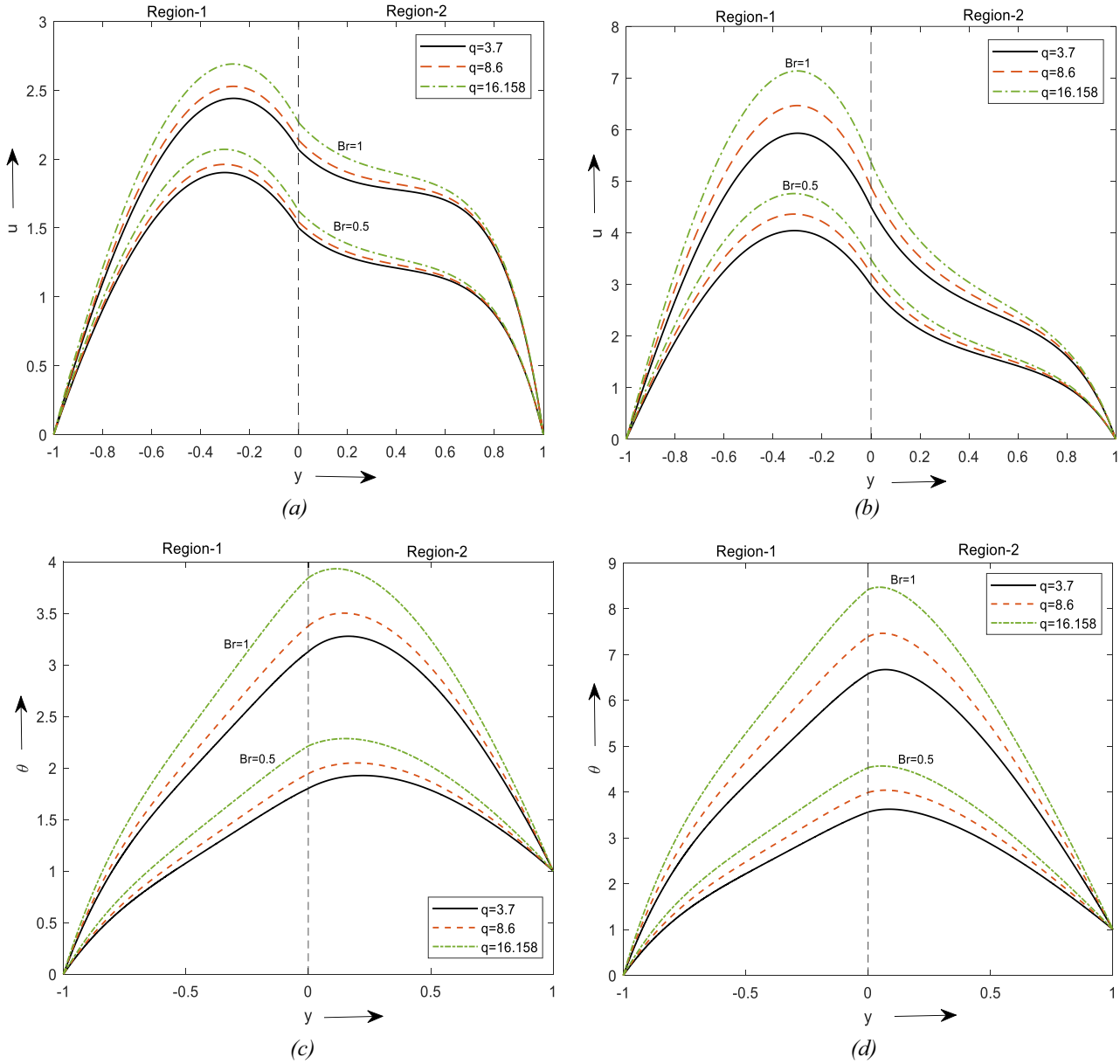

Figure 3. Velocity profiles for different values of Br. (**a**) For two different values of ϕ. (**b**) For a value of ϕ. Temperature profiles for different values of Br. (**c**) For two different values of ϕ. (**d**) For a value of ϕ.

is observed that the heat transfer rate and resistance to the flow increase with the augment of Br by keeping σ as constant. As Nu increases, heat transfers from the fluid to the wall. A similar observation can be made by keeping Br constant and varying σ.

Validation of the results. Prathap Kumar et al[58] considered a two-layer mixed convective flow of viscous fluid in a vertical channel with a chemical reaction. The governing equations Eqs. (1)–(7) of our study show good agreement with the literature of Prathap Kumar et al. in Eq. (2.1)–(2.7), in the absence of Nanofluids and Soret effect in our paper and chemical reaction in their paper. Table 3 shows the comparative study for different values of Brinkman number for velocity and temperature and Fig. 10 shows the comparison of the present work and Prathap Kumar et al. The results of our study are in a similar pattern to them, but not exactly equal to their result, as they have considered chemical reaction parameters to be unity (Supplementary file).

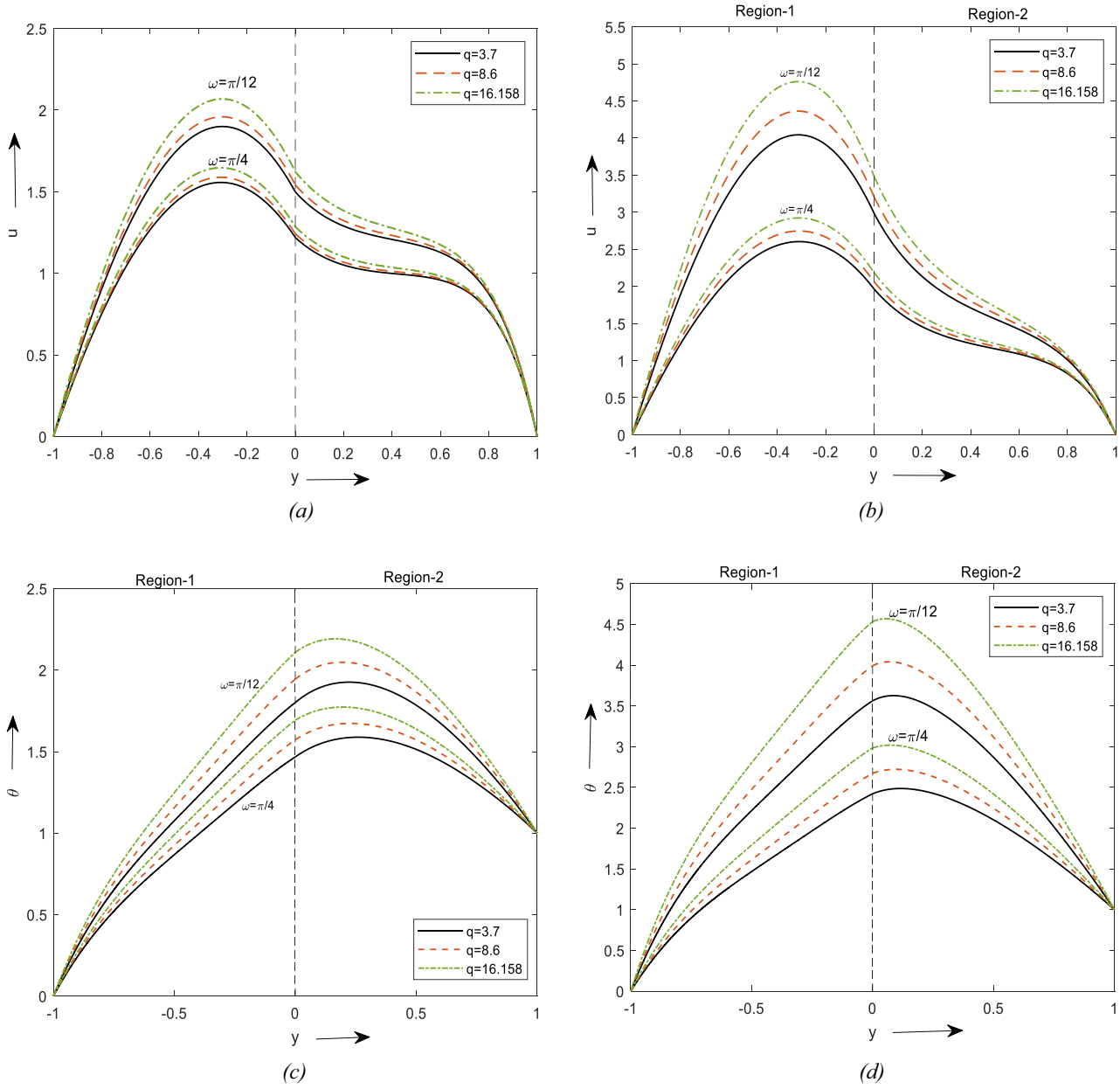

Figure 4. Velocity profiles for different values of ω. (**a**) For two different values of ϕ. (**b**) For a value of ϕ. Temperature profiles for different values of ω. (**c**) For two different values of ϕ. (**d**) For a value of ϕ.

Conclusion

- The fluids adjacent to the outer walls of the channel pass slowly, while the fluids with higher temperatures around the interface move with greater velocity.
- Current study shows that using a hybrid nanofluid is an important aspect of the cooling and heating process.
- From the graphs, it is noticed that the Grl and Br enhance the flow and temperature of the fluids, whereas the angle of inclination, and porosity of the medium downgrade.
- The effect of soret number can be significantly observed on velocity and concentration equations.
- A decrement in heat transfer rate at the hot plate and an increment at the cold plot are observed due to viscous dissipation.
- The effect of thermal diffusion is to increase the flow and heat transfer rate in the nanofluid region.
- The concentration of nanoparticles directly affects velocity and temperature in a manner of decreasing and increasing behaviour, respectively, due to their boundary layers.
- The comparison of velocity and temperature with Prathap Kumar et al.[58] shows that they are in good agreement (Table 3 and Fig. 10).

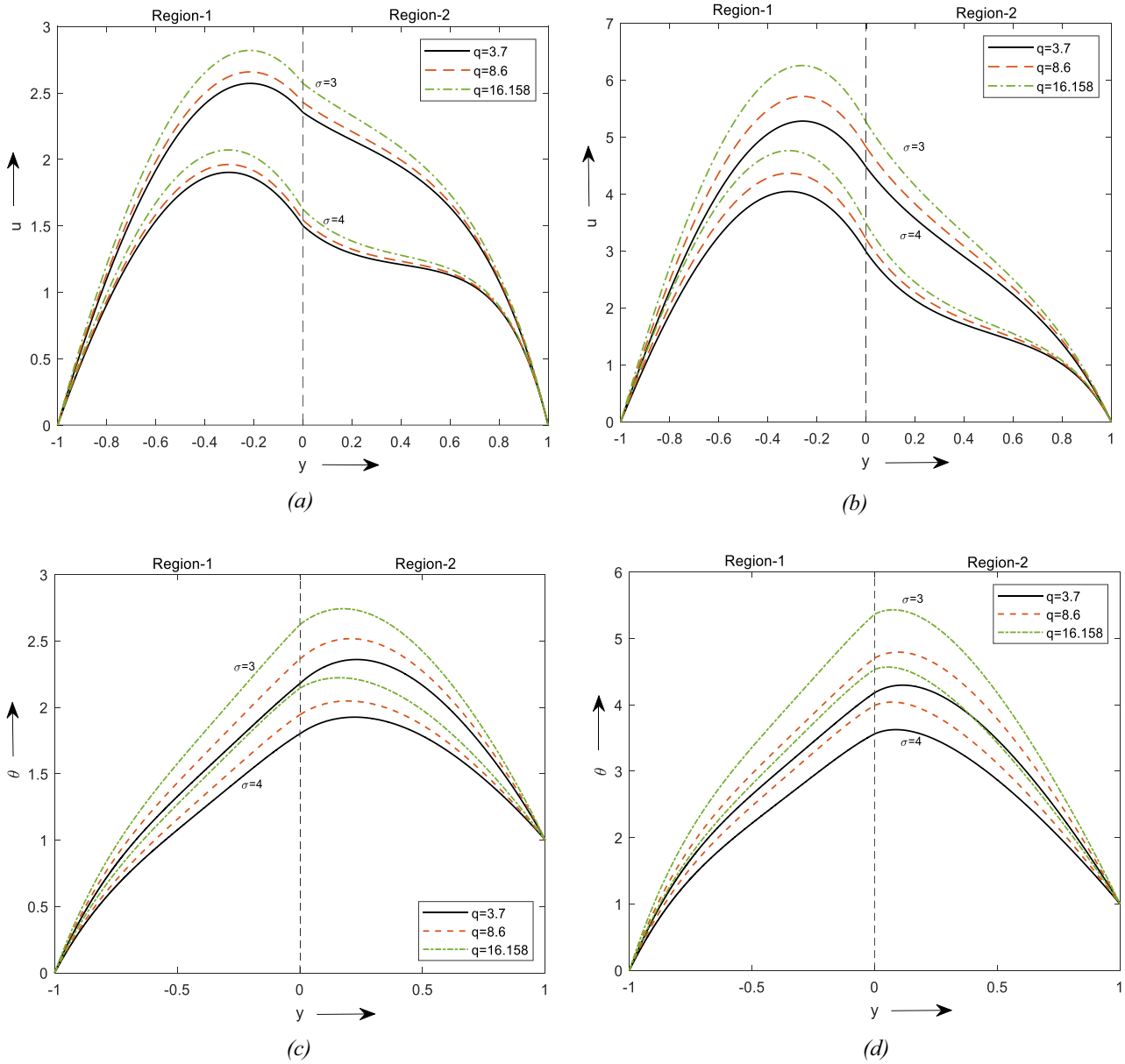

Figure 5. Velocity profiles for different values of σ. (**a**) For two different values of ϕ. (**b**) For a value of ϕ. Temperature profiles for different values of σ. (**c**) For two different values of ϕ. (**d**) For a value of ϕ.

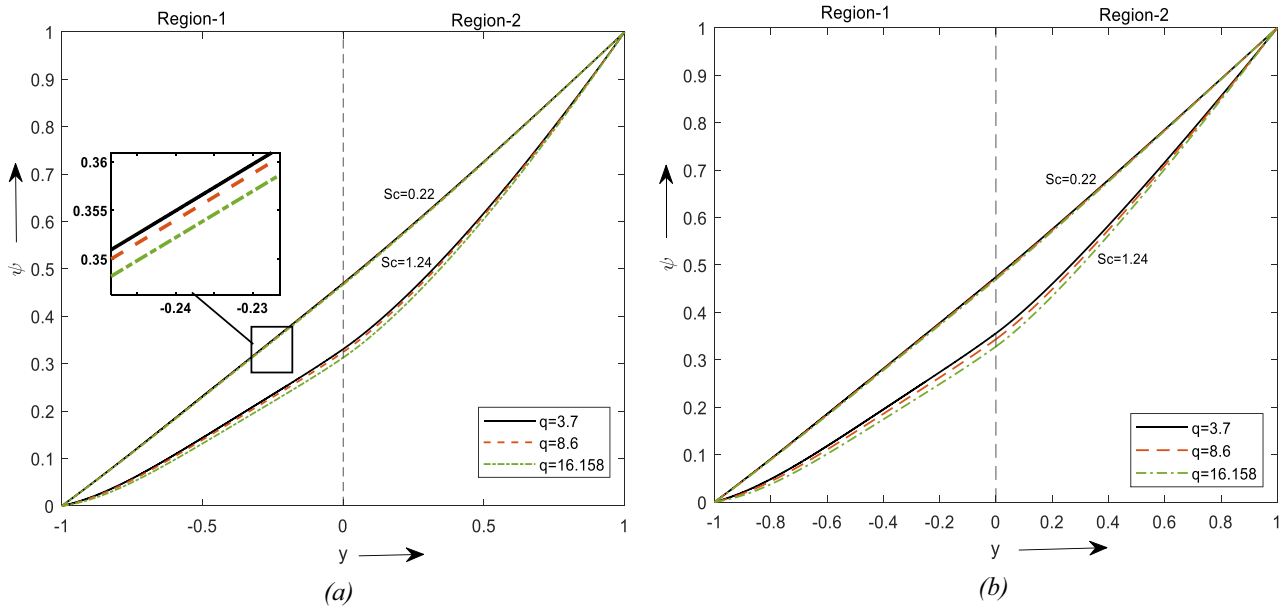

Figure 6. Concentration profiles for different values of Sc. (**a**) For two different values of ϕ. (**b**) For a value of ϕ.

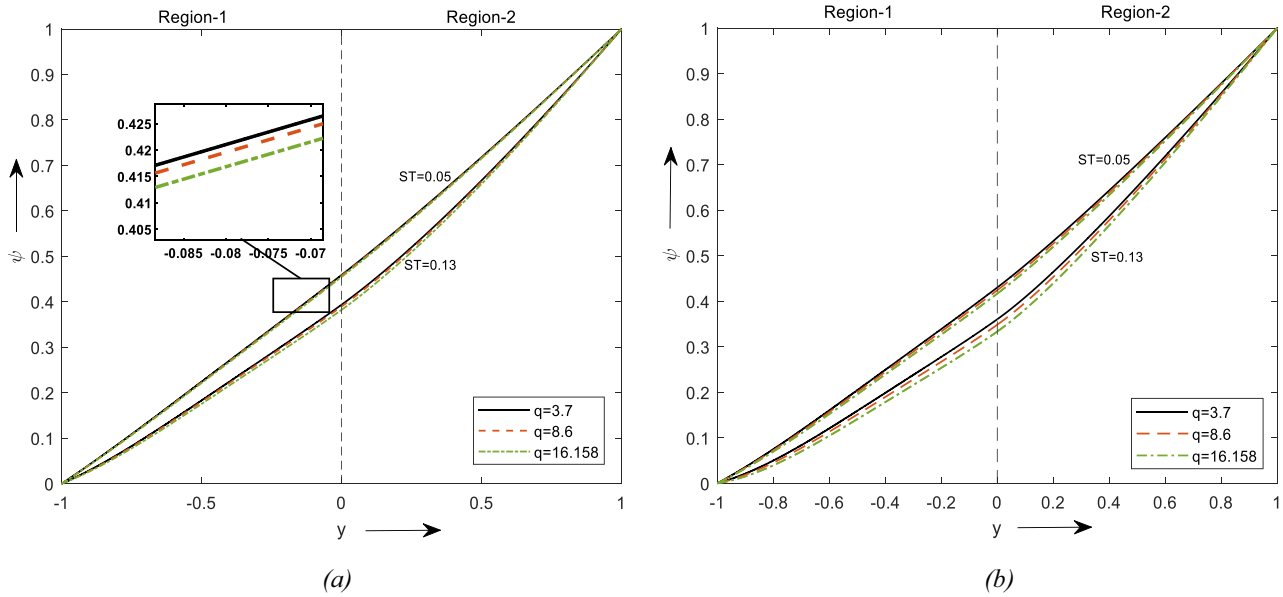

Figure 7. Concentration profiles for different values of ST. (**a**) For two different values of ϕ. (**b**) For a value of ϕ.

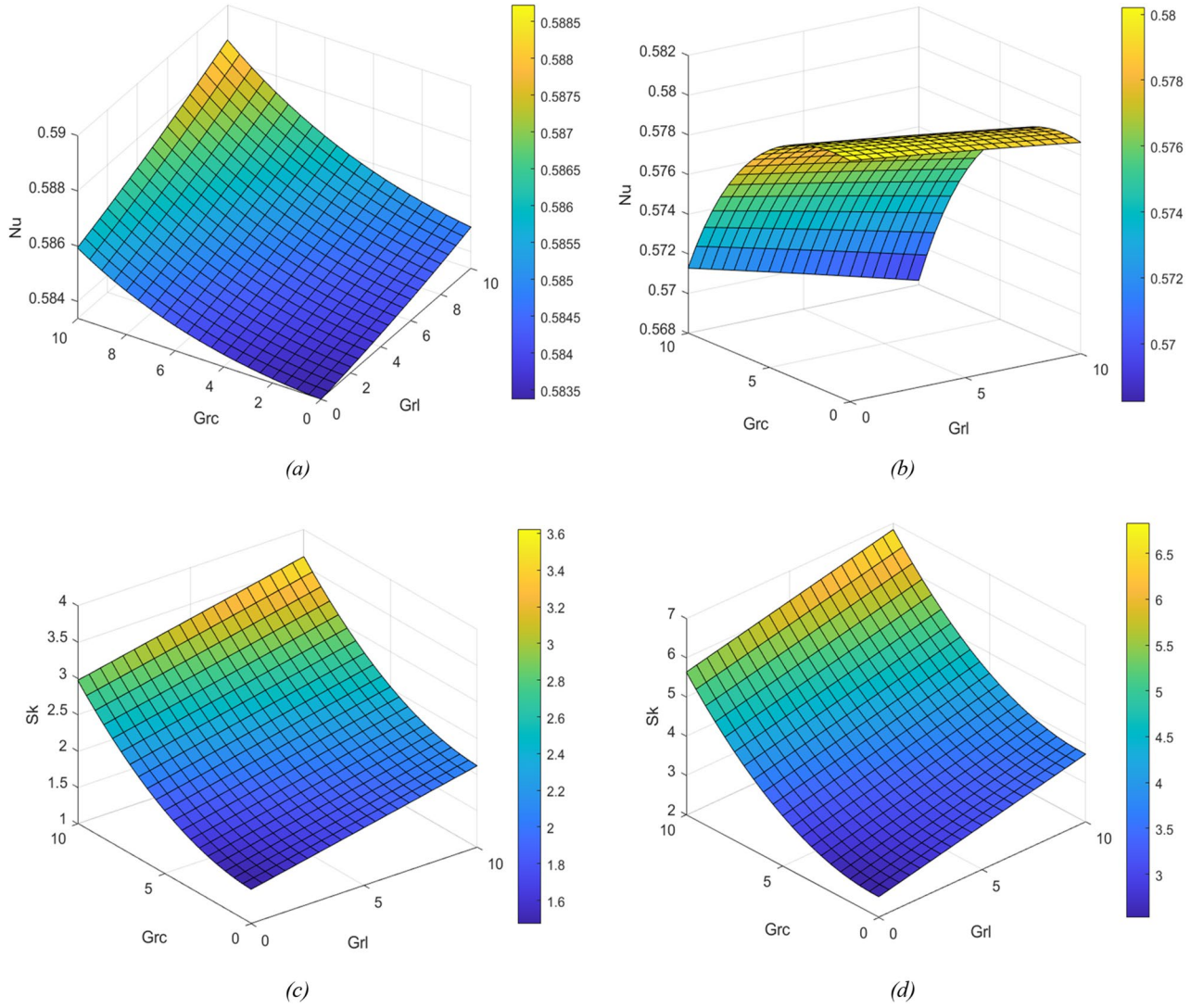

Figure 8. Nusselt graphs for change in GrL and GrC (**a**) at the left plate (y = − 1) (**b**) at the right plate (y = 1). Skin friction for change in GrL and GrC (**c**) at the left plate (y = − 1) (**d**) at the right plate (y = 1).

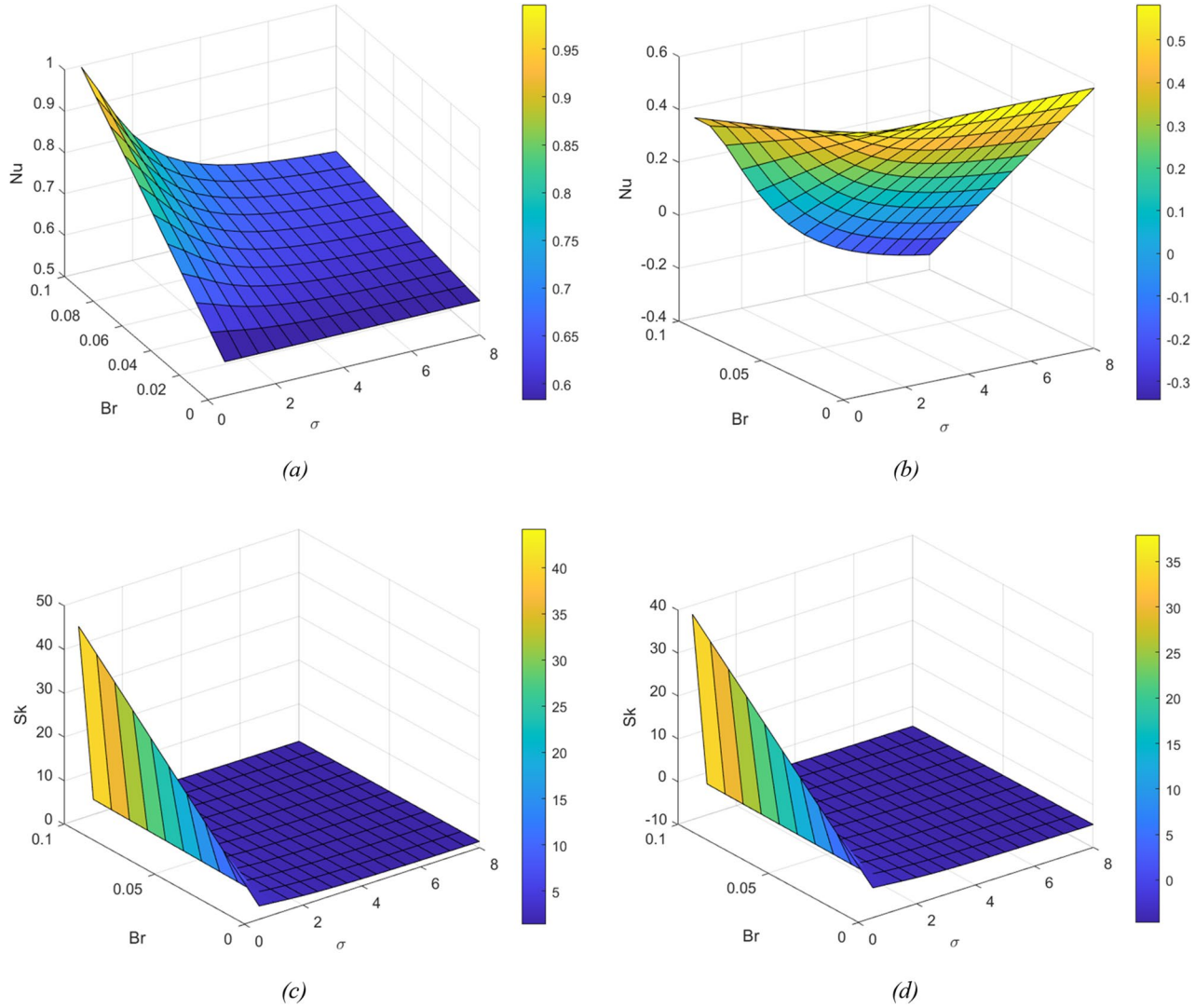

Figure 9. Nusselt graphs for change in Br and σ (**a**) at the left plate (y = − 1) (**b**) at the right plate (y =). Skin friction for change in Br and σ (**c**) at the left plate (y = − 1) (**d**) at the right plate (y = 1).

Temperature					Velocity				
	Br = 0		Br = 0.5			Br = 0		Br = 0.5	
y	Present	Prathap Kumar et al.[58]	Present	Prathap Kumar et al.[58]	y	Present	Prathap Kumar et al.[58]	Present	Prathap Kumar et al.[58]
− 1	0	0	0	0	− 1	0.0000	0.0000	0.0000	0.0000
− 0.8	0.1000	0.1000	0.1665	0.1790	− 0.8	0.2906	0.2905	0.3200	0.3128
− 0.6	0.2000	0.2000	0.3020	0.3219	− 0.6	0.5314	0.5347	0.5898	0.5763
− 0.4	0.3000	0.3000	0.4171	0.4407	− 0.4	0.7172	0.7265	0.8001	0.7824
− 0.2	0.4000	0.4000	0.5212	0.5459	− 0.2	0.8426	0.8591	0.9421	0.9239
0	0.5000	0.5000	0.6210	0.6458	0	0.9022	0.9260	0.9178	0.9938
0.2	0.6000	0.6000	0.7201	0.7447	0.2	0.8908	0.9198	0.9872	0.9849
0.4	0.7000	0.7000	0.8178	0.8421	0.4	0.8030	0.8329	0.8257	0.8894
0.6	0.8000	0.8000	0.9079	0.9303	0.6	0.6334	0.6570	0.6580	0.6992
0.8	0.9000	0.9000	0.9775	0.9924	0.8	0.3768	0.3828	0.4026	0.4057
1	1	1	1	1	1	0.0000	0.0000	0.0000	0.0000

Table 3. Fluid flow and temperature values for various values of Br.

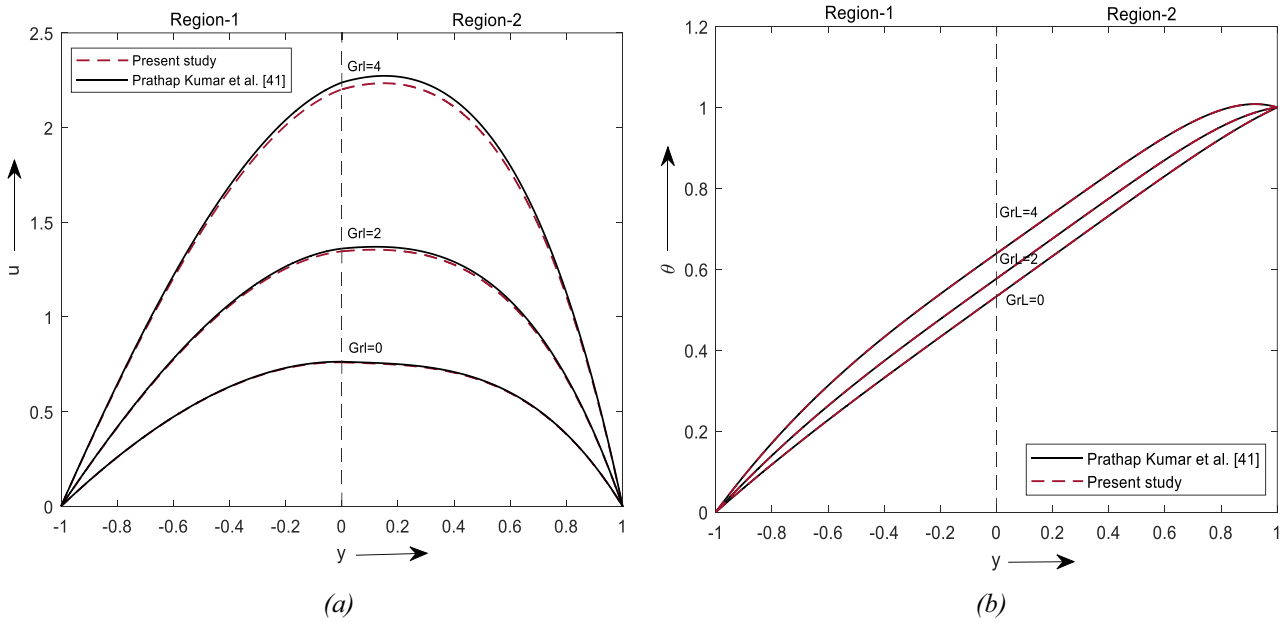

Figure 10. Comparison results of (**a**) velocity profile. (**b**) Temperature profile.

Data availability

The datasets used and/or analysed during the current study are available from the corresponding author upon reasonable request.

Received: 12 November 2022; Accepted: 12 December 2022
Published online: 18 December 2022

References

1. Choi, S. U. S. & Eastman, J. A. Enhancing thermal conductivity of fluids with nanoparticles. In *Proceedings of the 1995 ASME International Mechanical Engineering Congress and Exposition* 99–105 (1955).
2. Chamkha, A. J. Unsteady laminar hydromagnetic fluid-particle flow and heat transfer in channels and circular pipes. *Int. J. Heat Fluid Flow* **21**(6), 740–746 (2000).
3. Chamkha, A. J. On laminar hydromagnetic mixed convection flow in a vertical channel with symmetric and asymmetric wall heating conditions. *Int. J. Heat Mass Transf.* **45**(12), 2509–2525 (2002).
4. Abbasi, S., Zebarjad, S. M., Baghban, S. H. N., Youssefi, A. & Ekrami-Kakhki, M. S. Experimental investigation of the rheological behavior and viscosity of decorated multi-walled carbon nanotubes with TiO2 nanoparticles/water nanofluids. *J. Therm. Anal. Calorim.* **123**, 81–89 (2016).
5. Barbés, B., Páramo, R., Blanco, E. & Casanova, C. Thermal conductivity and specific heat capacity measurements of CuO nanofluids. *J. Therm. Anal. Calorim.* **115**, 1883–1891 (2014).
6. Shamshirband, S. *et al.* Performance investigation of micro- and nano-sized particle erosion in a 90° elbow using an ANFIS model. *Powder Technol.* **284**, 336–343 (2015).
7. Abd Elmaboud, Y. Two layers of immiscible fluids in a vertical semi-corrugated channel with heat transfer: Impact of nanoparticles. *Results Phys.* **9**, 1643–1655 (2018).
8. Bhattacharyya, A., Seth, G. S., Kumar, R. & Chamkha, A. J. Simulation of Cattaneo-Christov heat flux on the flow of single and multi-walled carbon nanotubes between two stretchable coaxial rotating disks. *J. Therm. Anal. Calorim.* **139**, 1655–1670 (2020).
9. Dogonchi, A. S., Nayak, M. K., Karimi, N., Chamkha, A. J. & Ganji, D. D. Numerical simulation of hydrothermal features of Cu–H2O nanofluid natural convection within a porous annulus considering diverse configurations of heater. *J. Therm. Anal. Calorim.* **141**, 2109–2125 (2020).
10. Selimefendigil, F., Öztop, H. F. & Chamkha, A. J. Role of magnetic field on forced convection of nanofluid in a branching channel. *Int. J. Numer. Methods Heat Fluid Flow* **30**, 1755–1772 (2020).
11. Toghraie, D. *et al.* Two-phase investigation of water-Al2O3 nanofluid in a micro concentric annulus under non-uniform heat flux boundary conditions. *Int. J. Numer. Methods Heat Fluid Flow* **30**, 1795–1814 (2020).
12. Parvin, S., Nasrin, R., Alim, M. A., Hossain, N. F. & Chamkha, A. J. Thermal conductivity variation on natural convection flow of water-alumina nanofluid in an annulus. *Int. J. Heat Mass Transf.* **55**, 5268–5274 (2012).
13. Nor, A. C. S. *et al.* Recent progress on hybrid nanofluids in heat transfer applications: A comprehensive review. *Int. Commun. Heat Mass Transfer* **78**, 68–79. https://doi.org/10.1016/j.icheatmasstransfer.2016.08.019 (2016).
14. Sundar, L. S., Sharma, K. V., Singh, M. K. & Sousa, A. C. M. Hybrid nanofluids preparation, thermal properties, heat transfer and friction factor—a review. *Renew. Sustain. Energy Rev.* **68**, 185–198. https://doi.org/10.1016/j.rser.2016.09.108 (2017).
15. Xian, H. W., Sidik, N. A. C. & Saidur, R. Impact of different surfactants and ultrasonication time on the stability and thermophysical properties of hybrid nanofluids. *Int. Commun. Heat Mass Transfer* **110**, 104389 (2020).
16. Prakash, D., Ragupathi, E., Muthtamilselvan, M., Abdalla, B. & Mdallal, Q. M. A. Impact of boundary conditions of third kind on nano liquid flow and radiative heat transfer through asymmetrical channel. *Case Stud. Therm. Eng.* **28**, 101488 (2021).
17. Jana, S., Salehi-Khojin, A. & Zhong, W. H. Enhancement of fluid thermal conductivity by the addition of single and hybrid nano-additives. *Thermochim. Acta* **462**, 45–55 (2007).
18. Niihara, K. New design concept of structural ceramics. *J. Ceram. Soc. Jpn.* **99**, 974–982 (1991).

19. Chamkha, A. J., Miroshnichenko, I. V. & Sheremet, M. A. Numerical analysis of unsteady conjugate natural convection of hybrid water-based nanofluid in a semicircular cavity. *J. Therm. Sci. Eng. Appl.* **9**, 4 (2017).
20. Ghalambaz, M., Sheremet, M. A., Mehryan, S. A. M., Kashkooli, F. M. & Pop, I. Local thermal non-equilibrium analysis of conjugate free convection within a porous enclosure occupied with Ag–MgO hybrid nanofluid. *J. Therm. Anal. Calorim.* **135**, 1381–1398 (2019).
21. Gokulavani, P., Muthtamilselvan, M., Abdalla, B. & Doh, D. H. Radiation effect of ND–Ni nanocomposite, water-filled multiport cavity with heated baffle. *Eur. Phys. J. Spec. Top.* **230**, 1201–1211 (2021).
22. Kanimozhi, B., Muthtamilselvan, M., Al-Mdallal, Q. M. & Abdalla, B. Double-diffusive buoyancy and marangoni convection in a hybrid nanofluid filled cylindrical porous annulus. *Microgravity Sci. Technol.* **34**, 17 (2022).
23. Suganya, S., Muthtamilselvan, M., Al-Amri, F. & Abdalla, B. An exact solution for unsteady free convection flow of chemically reacting Al2O3 – SiO2/ hybrid nanofluid. *Proc. Inst. Mech. Eng. C J. Mech. Eng. Sci.* **235**, 3749–3763 (2021).
24. Suganya, S., Muthtamilselvan, M. & Abdalla, B. Effects of radiation and chemical reaction on Cu–Al 2 O 3 /water hybrid flow past a melting surface in the existence of cross magnetic field. *Ricerche mat.* https://doi.org/10.1007/s11587-021-00606-z (2021).
25. Raza, J., Mebarek-Oudina, F. & Chamkha, A. J. Magnetohydrodynamic flow of molybdenum disulfide nanofluid in a channel with shape effects. *Multidiscipl. Model. Mater. Struct.* **15**, 737–757 (2019).
26. Sobamowo, M. G. Free convection flow and heat transfer of nanofluids of different shapes of nano-sized particles over a vertical plate at low and high Prandtl numbers. *J. Appl. Comput. Mech.* **5**, 13–39 (2019).
27. Hussain, A., Sarwar, L., Akbar, S., Nadeem, S. & Jamal, S. Numerical investigation of viscoelastic nanofluid flow with radiation effects. *Proc. Inst. Mech. Eng. Part N J. Nanomater. Nanoeng. Nanosyst.* **233**, 87–96 (2019).
28. Muneeshwaran, M., Srinivasan, G., Muthukumar, P. & Wang, C. C. Role of hybrid-nanofluid in heat transfer enhancement—a review. *Int. Commun. Heat Mass Transfer* **125**, 105341 (2021).
29. Chamkha, A. J. Non-darcy fully developed mixed convection in a porous medium channel with heat generation/absorption and hydromagnetic effects. *Numer. Heat Transf. A Appl.* **32**, 653–675 (1997).
30. Alomar, O. R., Aslan, S. R. & Zaki, F. G. Modelling and simulation of two-phase flow inside porous pipe evaporator using Cu-Water nano-fluid. *Int. J. Therm. Sci.* **175**, 107462 (2022).
31. Wang, L., Lu, Y., Qi, Y. & Wang, M. Study on the mass and heat transfer of gas-liquid two-phase flow in the porous media based on the 3D reconstruction model. *Powder Technol.* **393**, 143–153 (2021).
32. Aminian, E., Moghadasi, H. & Saffari, H. Magnetic field effects on forced convection flow of a hybrid nanofluid in a cylinder filled with porous media: A numerical study. *J. Therm. Anal. Calorim.* **141**, 2019–2031 (2020).
33. Bég, O. A., Zaman, A., Ali, N., Gaffar, S. A. & Bég, E. T. Numerical computation of nonlinear oscillatory two-immiscible magnetohydrodynamic flow in dual porous media system: FTCS and FEM study. *Heat Transfer Asian Res.* **48**, 1245–1263 (2019).
34. Chamkha, A. J. Pergamon hydromagnetic two-phase flow in a channel. *Int. J. Eng. Sci.* **1995**, 33 (1995).
35. Khaled, A. R. A. & Vafai, K. Heat transfer enhancement by layering of two immiscible co-flows. *Int. J. Heat Mass Transf.* **68**, 299–309 (2014).
36. Umavathi, J. C. & Anwar-Bég, O. Effects of thermophysical properties on heat transfer at the interface of two immisicible fluids in a vertical duct: Numerical study. *Int. J. Heat Mass Transf.* **154**, 52 (2020).
37. Chen, X. & Jian, Y. Entropy generation minimization analysis of two immiscible fluids. *Int. J. Therm. Sci.* **171**, 526 (2022).
38. Malashetty, M. S., Umavathi, J. C. & Kumar, J. P. Magnetoconvection of two-immiscible fluids in vertical enclosure. *Heat Mass Transfer* **42**, 977–993 (2006).
39. Chamkha, A. J. *Flow of Two-Immiscible Fluids in Porous and Nonporous Channels*. http://fluidsengineering.asmedigitalcollection.asme.org/ (2000).
40. Sheikholeslami, M., Hatami, M. & Domairry, G. Numerical simulation of two phase unsteady nanofluid flow and heat transfer between parallel plates in presence of time dependent magnetic field. *J. Taiwan Inst. Chem. Eng.* **46**, 43–50 (2015).
41. Rahim, T., Abbas, Z., Abid, N. & Hasnain, J. Heat transfer enhancement in oscillatory two-phase flow of Casson and ferrofluid comprising differently shaped nanoparticles in a horizontal composite channel. *Heat Transfer* **50**, 7733–7763 (2021).
42. Chandrawat, R. K. & Joshi, V. Numerical study of ion-slip and hall effect on couette flow of two immiscible micropolar and micropolar dusty fluid (fluid-particle suspension) with heat transfer. *Int. J. Heat Technol.* **39**, 1180–1196 (2021).
43. Abbas, Z., Altaf, I., Hasnain, J. & Ali, A. Theoretical analysis of two-layer fluids with continuity of stresses at interface and slip at the walls of an inclined channel. *Ain Shams Eng. J.* **12**, 761–774 (2021).
44. Kumar, J. P., Umavathi, J. C., Chamkha, A. J. & Pop, I. Fully-developed free-convective flow of micropolar and viscous fluids in a vertical channel. *Appl. Math. Model.* **34**, 1175–1186 (2010).
45. Umavathi, J. C., Chamkha, A. J., Mateen, A. & Al-Mudhaf, A. Unsteady two-fluid flow and heat transfer in a horizontal channel. *Heat Mass Transf.* **42**, 81–90 (2005).
46. Tritton, D. J. *Physical Fluid Dynamics* (Van Nostrand Reinhold Co, 1977).
47. Sheikholeslami, M. & Bhatti, M. M. Forced convection of nanofluid in presence of constant magnetic field considering shape effects of nanoparticles. *Int. J. Heat Mass Transf.* **111**, 1039–1049 (2017).
48. Shoaib, M. *et al.* Numerical investigation for rotating flow of MHD hybrid nanofluid with thermal radiation over a stretching sheet. *Sci. Rep.* **10**, 18533 (2020).
49. Tiwari, R. K. & Das, M. K. Heat transfer augmentation in a two-sided lid-driven differentially heated square cavity utilizing nanofluids. *Int. J. Heat Mass Transf.* **50**, 2002–2018 (2007).
50. Darcy, H. *Les Fontaines Publiques de la Ville de Dijon* (Dalmont, 1856).
51. Chamkha, A. J. Non-Darcy hydromagnetic free convection from a cone and a wedge in porous media. *Int. Commun. Heat Mass Transfer* **23**, 875–887 (1996).
52. Chamkha, A. J. & Ben-Nakhi, A. MHD mixed convection–radiation interaction along a permeable surface immersed in a porous medium in the presence of Soret and Dufour's Effects. *Heat Mass Transf.* **44**, 845–856 (2008).
53. Ghasemi, B. & Aminossadati, S. M. Natural convection heat transfer in an inclined enclosure filled with a water-cuo nanofluid. *Numer. Heat Transf. A Appl.* **55**, 807–823 (2009).
54. Muthtamilselvan, M., Kandaswamy, P. & Lee, J. Heat transfer enhancement of copper-water nanofluids in a lid-driven enclosure. *Commun. Nonlinear Sci. Numer. Simul.* **15**, 1501–1510 (2010).
55. Vajravelu, K., Prasad, K. V. & Abbasbandy, S. Convective transport of nanoparticles in multi-layer fluid flow. *Appl. Math. Mech.* **34**, 177–188 (2013).
56. Maxwell, J. *A Treatise on Electricity and Magnetism* (Oxford University Press, 1904).
57. Brinkman, H. C. The viscosity of concentrated suspensions and solutions. *J. Chem. Phys.* **20**, 571–571 (1952).
58. Kumar, J. P., Umavathi, J. C. & Kalyan, S. Chemical reaction effects on mixed convection flow of two immiscible viscous fluids in a vertical channel. *Open J. Heat Mass Moment. Transfer* **2**, 28 (2014).

Acknowledgements

The work was supported by the research seed grant Ref no:RU:EST: MT:2022/4 funded by REVA University.

Competing interests
The authors declare no competing interests.

Additional information
Supplementary Information The online version contains supplementary material available at https://doi.org/10.1038/s41598-022-26169-z.

Correspondence and requests for materials should be addressed to M.H.

Reprints and permissions information is available at www.nature.com/reprints.

Publisher's note Springer Nature remains neutral with regard to jurisdictional claims in published maps and institutional affiliations.